J|A|C|S
ARTICLES
Published on Web 05/21/2005

Generalized Synthesis of Metal Phosphide Nanorods via Thermal Decomposition of Continuously Delivered Metal−Phosphine Complexes Using a Syringe Pump

Jongnam Park,[†] Bonil Koo,[†] Ki Youl Yoon,[†] Yosun Hwang,[‡] Misun Kang,[‡] Je-Geun Park,[‡] and Taeghwan Hyeon*,[†]

Contribution from the National Creative Research Center for Oxide Nanocrystalline Materials and the School of Chemical and Biological Engineering, Seoul National University, Seoul 151-744, Korea, and Department of Physics and Institute of Basic Science, Sungkyunkwan University, Suwon 440-746, Korea

Received December 2, 2004; E-mail: thyeon@plaza.snu.ac.kr

Abstract: We synthesized uniform-sized nanorods of transition metal phosphides from the thermal decomposition of continuously delivered metal-phosphine complexes using a syringe pump. MnP nanorods with dimensions of 8 nm × 16 nm and 6 nm × 22 nm sized were synthesized by the thermal decomposition of Mn−TOP complex, which was prepared from the reaction of $Mn_2(CO)_{10}$ and tri-*n*-octylphosphine (TOP), using a syringe pump with constant injection rates of 10 and 20 mL/h, respectively. When Co−TOP complex, which was prepared from the reaction of cobalt acetylacetonate and TOP, was reacted in a mixture solvent composed of octyl ether and hexadecylamine at 300 °C using a syringe pump, uniform 2.5 nm × 20 nm sized Co_2P nanorods were generated. When cobaltocene was employed as a precursor, uniform Co_2P nanorods with 5 nm × 15 nm were obtained. When Fe−TOP complex was added to trioctylphosphine oxide (TOPO) at 360 °C using a syringe pump and then allowed to age at 360 °C for 30 min, uniform-sized FeP nanorods with an average dimension of 12 nm × 500 nm were produced. Nickel phosphide (Ni_2P) nanorods with 4 nm × 8 nm were synthesized successfully by thermally decomposing the Ni−TOP complex, which was synthesized by reacting acetylacetonate [$Ni(acac)_2$] and TOP. We measured the magnetic properties of these nanorods, and some of the nanorods exhibited different magnetic characteristics compared to the bulk counterparts.

Introduction

Uniformly sized one-dimensional (1-D) nanostructures, such as nanorods, nanowires, and nanotubes, have received much attention because of the unique properties derived from their dimensional anisotropy and their potential applications as interconnectors and functional building blocks for nanodevices.[1] There are various strategies for obtaining 1-D nanostructured materials that include the use of intrinsically anisotropic crystal structures, structure-directing soft or hard templates, different coordinating ligands to control the growth rates of different facets, the vapor−liquid−solid process, and the self-assembly of spherical nanoparticles by oriented attachment.[2] These methods have successfully achieved 1-D nanostructured metals,[3] metal chalcogenides,[4] and metal oxides.[5] However, efforts to prepare 1-D metal phosphide nanostructures are rare despite their scientific and technological importance. Nanostructured metal phosphides are currently of great interest in chemistry and materials sciences, because they exhibit various interesting properties, including ferromagnetism, semiconductivity, catalytic and magnetocaloric properties, and magnetoresistance.[6] In

[†] Seoul National University.
[‡] Sungkyunkwan University.

(1) (a) A special issue on nanowires: *Adv. Mater.* **2003**, *15*, 351. (b) Cui, Y.; Lieber, C. M. *Science* **2001**, *291*, 851. (c) Hanrath, T. T.; Korgel, B. A. *J. Am. Chem. Soc.* **2001**, *124*, 1424. (d) Schmid, G. *Nanoparticles: From Theory to Application*; Wiley-VCH: Weinheim 2004. (e) Klabunde, K. J. *Nanoscale Materials in Chemistry;* Wiley-Interscience: New York, 2001. (f) Fendler, J. H. *Nanoparticles and Nanostructured Films;* Wiley-VCH: Weinheim, 1998. (g) Alivisatos, A. P. *Science* **1996**, *271*, 933. (h) Pacholski, C.; Kornowsli, A.; Weller, H. *Angew. Chem., Int. Ed.* **2002**, *41*, 1188. (i) Hyeon, T. *Chem. Commun.* **2003**, 927.
(2) Xia, Y.; Yang, P.; Sun, Y.; Wu, Y.; Mayers, B.; Gates, B.; Yin, Y.; Kim, F.; Yan, H. *Adv. Mater.* **2003**, *15*, 353.
(3) (a) Dumestre, F.; Chaudret, B.; Amiens, C.; Respaud, M.; Fejes, P.; Renaud, P.; Zurcher, P. *Angew. Chem. Int. Ed.* **2003**, *42*, 5213. (b) Dumestre, F.; Chaudret, B.; Amiens, C.; Fromen, M.-C.; Casanove, M.-J.; Respaud, M.; Zurcher, P. *Angew. Chem., Int. Ed.* **2002**, *41*, 4286. (c) Cordente, N.; Respaud, M.; Senocq, F.; Casanove, M. J.; Amiens, C.; Chaudret, B. *Nano Lett.* **2001**, *1*, 565. (d) Puntes, V. F.; Krishnan, K. M.; Alivisatos, A. P. *Science* **2001**, *291*, 2115. (e) Puntes, V. F.; Zanchet, D.; Erdonmez, C. K.; Alivisatos, A. P. *J. Am. Chem. Soc.* **2002**, *124*, 12874. (f) Park, S.-J.; Kim, S.; Lee, S.; Khim, Z. G.; Char, K.; Hyeon, T. *J. Am. Chem. Soc.* **2000**, *122*, 8581. (g) Song, J. H.; Wu, Y.; Messer, B.; Kind, H., Yang, P. *J. Am. Chem. Soc.* **2001**, *123*, 10397.
(4) (a) Sigman, M. B., Jr.; Ghezelbash, A.; Hanrath, T.; Saunders: A. E.; Lee, F.; Korgel, B. A. *J. Am. Chem. Soc.* **2003**, *125*, 16050. (b) Larsen, T. H.; Sigman, M.; Ghezelbash, A.; Doty, R. C.; Korgel, B. A. *J. Am. Chem. Soc.* **2003**, *125*, 5638. (c) Gudiksen, M. S.; Lieber, C. M. *J. Am. Chem. Soc.* **2000**, *122*, 8801. (d) Gudiksen, M. S.; Wang, J.; Lieber, C. M. *J. Phys. Chem. B* **2001**, *105*, 4062. (e) Barrelet, C. J.; Wu, Y.; Bell, D. C.; Lieber, C. M. *J. Am. Chem. Soc.* **2003**, *125*, 11498. (f) Wu, Y.; Yan, H.; Huang, M.; Messer, B.; Song, J. H.; Yang, P. *Chem. Eur. J.* **2002**, *8*, 1261. (g) Peng, Z. A.; Peng, X. *J. Am.* Chem. Soc. **2001**, *123*, 183. (h) Tang, Z.; Kotov, N. A.; Giersig, M. *Science* **2002**, *297*, 237. (i) Nath, M.; Choudhury, A.; Kundu, A.; Rao, C. N. R. *Adv. Mater.* **2003**, *15*, 2098. (j) Manna, L.; Milliron, D. J.; Meisel, A.; Scher, E. C.; Alivisatos, A. P. *Nature. Mater.* **2003**, *2*, 382. (k) Lee, S.-M.; Cho, S.-N.; Cheon, J. *Adv. Mater.* **2003**, *15*, 441. (l) Hu, J.; Bando, Y.; Liu, Z.; Ahan, J.; Golberg, D.; Sekiguchi, T. *Angew. Chem., Int. Ed.* **2004**, *43*, 63.

addition, they are promising materials for data storage devices, magnetic refrigeration systems, and hard drive read heads. Although it is very interesting to investigate the shape-dependent properties of nanostructured metal phosphides, they have been poorly explored because of the lack of appropriate and generalized synthetic methodologies. Recently, Brock et al. synthesized many spherical metal phosphide nanoparticles.[7] They showed that phosphine surfactants can serve as both stabilizing ligands and as phosphorus source. Recently, Liu and co-workers synthesized well-defined FeP nanorods and nanowires by the multiple injection of iron pentacarbonyl and phosphine mixtures.[8] We recently reported on the synthesis of uniformly sized magnetic Fe_2P nanorods from the thermal decomposition of continuously delivered iron−phosphine complex using a syringe pump.[9] By controlling the injection rate and by using different surfactants, we were able to control the diameters and aspect ratios of the nanorods. We further extended this procedure, and here we report on the generalized syntheses of various metal phosphides nanorods.

Experimental Section

Chemicals. Hexane, ethanol, and acetone were distilled and degassed before use. Dimanganese decacarbonyl ($Mn_2(CO)_{10}$, 98%), dicobalt octacarbonyl [$Co_2(CO)_8$, stabilized with 1−5% of hexane], and cyclopentadienylcobalt dicarbonyl [$C_5H_5Co(CO)_2$, 95%] were purchased from Strem Chemicals. Manganese acetylacetonate [$Mn(acac)_2$], cobalt acetylacetonate [$Co(acac)_2$, 97%], bis(cyclopentadienyl)cobalt [cobaltocene, $(C_5H_5)_2Co$], tri-*n*-octylphosphine (TOP, 90%), trioctylphosphine oxide (TOPO, 90%), hexadecylamine (HDA, 90%), octyl ether (OE, 99%), nickel acetylacetonate [$Ni(acac)_2$, 97%], and iron pentacarbonyl [$Fe(CO)_5$, 99.999%] were purchased from Aldrich Chemicals. TOPO was purified by vacuum distillation before use.

Synthesis of MnP Nanorods. Unless otherwise noted, all reactions were carried out in a dry argon atmosphere using a glovebox or standard Schrenk line techniques. In a typical synthesis, a Mn−TOP complex stock solution was prepared by mixing 0.148 g of $Mn_2(CO)_{10}$ (0.38 mmol) and 5 mL of TOP at 70 °C. The Mn−TOP complex solution was continuously supplied to 5 g of TOPO solution under vigorous stirring at 330 °C via a syringe pump. Smoke evolution and a color change from deep yellow to black occurred within a few minutes after injecting the stock solution, indicating that nuclei were generated by the thermal decomposition of the Mn−TOP complex. The resulting solution was maintained at 330 °C for 1 h and cooled to about 60 °C. The addition of 50 mL of anhydrous ethanol or acetone to the solution resulted in the flocculation of the nanorods. The flocculate was separated from the supernatant by centrifugation, and washed twice with 50 mL of ethanol to remove excess TOP and TOPO. The final precipitate was vacuum-dried and obtained as a powder. The manganese phosphide nanorods produced were found to be readily dispersible in organic solvents such as hexane, toluene, or chloroform.

Synthesis of Co_2P Nanorods. Cobalt phosphide nanorods were synthesized using a similar procedure as that described above for MnP nanorods. In a typical synthesis, a Co−TOP complex stock solution was prepared by reacting 0.27 g of $Co(acac)_2$ (0.98 mmol) and 10 mL of tri-*n*-octylphosphine (TOP) at 70 °C. The color of the solution changed from pink to violet after the complete dissolution of the cobalt acetylacetonate, indicating the formation of a Co−TOP complex. This stock solution was continuously delivered to a round-bottomed flask containing 10 mL of octyl ether (OE) and 1.47 g of hexadecylamine (HDA) at 300 °C using a syringe pump. The resulting solution was kept at 300 °C for 1 h. Co_2P nanorods were separated by adding 50 mL of ethanol followed by centrifugation. The collected black powder was also dispersible in many organic solvents.

Synthesis of FeP Nanorods. Fe−TOP complex solution, which was prepared by reacting 0.2 mL of $Fe(CO)_5$ (1.52 mmol) and 10 mL of TOP at 50 °C, was added to 5 g of TOPO at 360 °C using a syringe pump at the rate of 10 mL/h under a vigorous stirring. The resulting solution was further aged at 360 °C for 30 min, producing FeP nanorods. FeP nanorods were obtained in powder form by adding 50 mL of ethanol followed by centrifugation.

Synthesis of Ni_2P Nanorods. Ni−TOP complex stock solution, prepared by reacting 0.19 g of $Ni(acac)_2$ (0.72 mmol) and 10 mL of TOP at 60 °C, was continuously added to 5 g of TOPO solution with vigorous stirring at 330 °C via a syringe pump. The resulting solution was maintained at 330 °C for 1 h. The reaction was stopped by cooling to ∼60 °C. The solution was then treated with 50 mL of ethanol, to form a black brown precipitate. Ni_2P nanorods powder was obtained from the supernatant by centrifugation.

Characterization of Materials. Metal phosphide nanorods were characterized by low- and high-resolution transmission electron microscopy (TEM), electron diffraction (ED), and X-ray diffraction (XRD). TEM images were collected on a JEOL JEM-2010 electron microscope operating at 200 kV. Samples for TEM analysis were prepared by putting a drop of organic solution containing the nanorods on the surface of a copper grid coated with an amorphous carbon film. XRD patterns were obtained using a Rigaku D/Max-3C diffractometer equipped with a rotation anode and a Cu Kα radiation source (λ = 0.154 18 nm). The magnetic properties of the metal phosphide nanorods were characterized using a magnetic property measurement system (MPMS) 5XL Quantum design SQUID magnetometer in the temperature range 5−300 K. The KDS 100 syringe pump was employed for continuous and well-controlled release of metal−surfactant complex.

Results and Discussion

Metal phosphide nanorods were synthesized by the solution-phase thermal decomposition of continuously delivered metal−phosphine complexes using a syringe pump in a hot surfactant solution.[9] A syringe pump was employed to ensure the continuous and constant delivery of metal−phosphine complex into hot surfactant solution, thus inducing thermal decomposition and one-dimensional nanorod growth. When single or multiple injections of metal−phosphine complexes were performed without a syringe pump, polydisperse spherical nanoparticles or nonuniform-sized nanorods were produced. In addition, nanorod lengths were easily controlled by varying injection rates. Figure 1 represents a schematic illustration of the experimental setup employed for the synthesis of uniformly sized nanorods using a syringe pump.

Synthesis of MnP Nanorods. Figure 2, parts a and c, shows the 8 nm × 16 nm and 6 nm × 22 nm sized MnP nanorods that

(5) (a) Zhang, D.; Liu, Z.; Han, S.; Li, C.; Lei, B.; Stewart, M. P.; Tour, J. M.; Zhou, C. *Nano Lett.* **2004**, *11*, 2151. (b) Woo, K.; Lee, H. J.; Ahn, J.-P.; Park, Y. S. *Adv. Mater.* **2003**, *15*, 1761. (c) Lee, K.; Seo, W. S.; Park, J. T. *J. Am. Chem. Soc.* **2003**, *125*, 3408. (d) Wang, J.; Chen, Q.; Zeng, C.; Hou, B. *Adv. Mater.* **2004**, *16*, 137. (e) Urban, J. J.; Yun, W. S.; Gu, Q.; Park, H. *J. Am. Chem. Soc.* **2002**, *124*, 1186. (f) Pacholski, C.; Kornowski, A.; Weller, H. *Angew. Chem., Int. Ed.* **2002**, *41*, 1188. (g) Gu, G.; Zheng, B.; Han, W. Q.; Roth, S.; Liu, J. *Nano Lett.* **2002**, *2*, 849.
(6) (a) Arinsson, B.; Landstrom, T.; Rundquist, S. *Borides, Silicides and Phosphides*; Wiley: New York, 1965. (b) Greenwood, N. N.; Earnshaw, A. *Chemistry of the Elements*; Pergamon Press: New York, 1994. (c) Stinner, C.; Prins, R.; Weber, Th. *J. Catal.* **2001**, *202*, 187. (d) Oyama, S. T. *J. Catal.* **2003**, *216*, 343. (e) Muetterties, E. L.; Sauer, J. C. *J. Am. Chem. Soc.* **1974**, *96*, 3410. (f) Lukehart, C. M.; Milne, S. B.; Stock, S. R. *Chem. Mater.* **1988**, *10*, 903. (g) Luo, F.; Su, H.-L.; Song, W.; Wang, Z.-M.; Yan, Z.-G.; Yan, C.-H. *J. Mater. Chem.* **2004**, *14*, 111. (h) Tegus, O.; Bruck, E.; Buschow, K. H. J.; de Boer, F. R. *Nature* **2002**, *415*, 150.
(7) (a) Perera, S. C.; Tsoi, G.; Wenger, L. E.; Brock, S. L. *J. Am. Chem. Soc.* **2003**, *125*, 13960. (b) Stamm, K. L.; Garno, J. C.; Liu, G.-y.; Brock, S. L. *J. Am. Chem. Soc.* **2003**, *125*, 4038.
(8) Qian, C.; Kim, F.; Ma, L.; Tsui, F.; Yang, P.; Liu, J. *J. Am. Chem. Soc.* **2004**, *126*, 1195.
(9) Park, J.; Koo, B.; Hwang, Y.; Bae, C.; An, K.; Park, J.-G.; Park, H. M.; Hyeon, T. *Angew. Chem., Int. Ed.* **2004**, *43*, 2282.

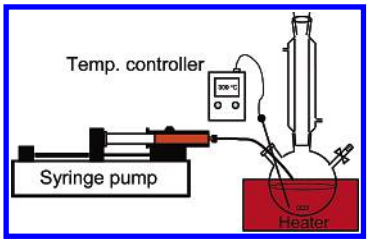

Figure 1. Schematic illustration of the experimental setup for the synthesis of uniformly sized nanorods.

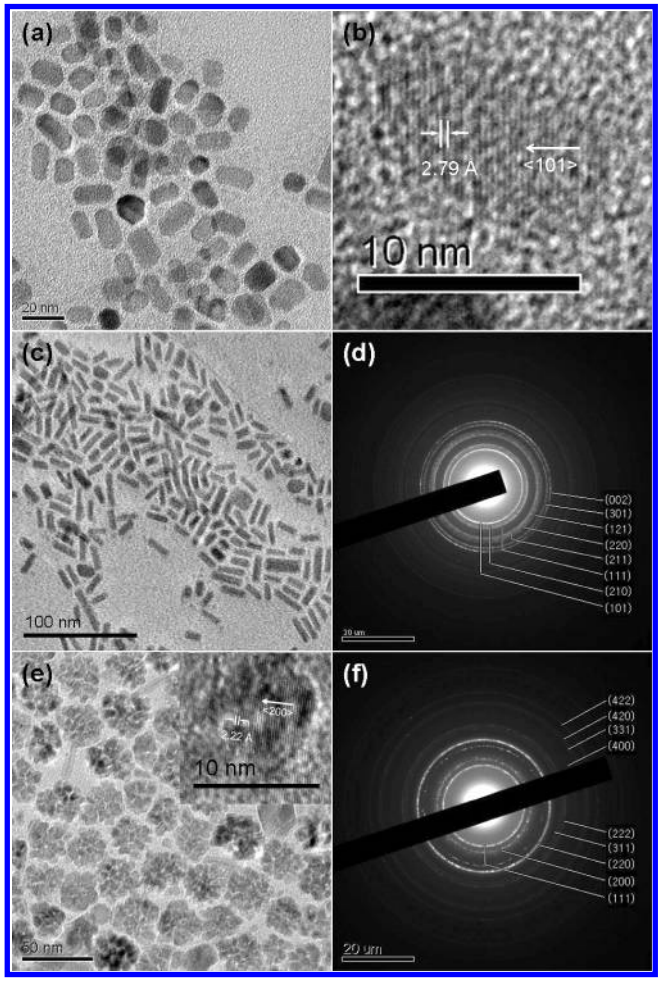

Figure 2. (a) Normal TEM and (b) high-resolution TEM images of 8 nm × 16 nm sized MnP nanorods, obtained using an injection rate of 10 mL/h, (c) TEM image and (d) electron diffraction patterns of 6 nm × 22 nm sized MnP nanorods, obtained using an injection rate of 20 mL/h, and (e) TEM image and (f) electron diffraction patterns of 5 nm sized MnO nanoparticles. The inset of panel e is a high-resolution TEM of MnO nanoparticles.

were synthesized by the thermal decomposition of Mn−TOP complex, which was prepared from the reaction of $Mn_2(CO)_{10}$ and tri-*n*-octylphosphine (TOP), using a syringe pump with constant injection rates of 10 and 20 mL/h, respectively. The high-resolution transmission electron microscope (HRTEM) image of the 8 nm × 16 nm sized MnP nanorods showed a distinct lattice fringe, indicative of a highly crystalline nature (Figure 2b). The length of the MnP nanorods was directly proportional to the injection rate of the Mn−TOP complex. This trend was contrary to our previous experiences of the synthesis of Fe_2P nanorods from the thermal decomposition of syringe pump delivered Fe−TOP complex, where longer nanorods were produced at lower injection rates. In the syntheses of the MnP nanorods, Mn−TOP complex was found to be highly stable and could be decomposed above a certain precursor concentration. When 0.76 mmol of Mn−TOP solution was added to a TOPO solution at 330 °C at a high injection rate of 20 mL/h via a syringe pump, the color of the reaction mixture turned to dark brown after ~8 min, indicating that nucleation occurred by the thermal decomposition of the Mn−TOP complex. After the reaction was complete, thin long MnP nanorods of dimension 6 nm (diameter) × 22 nm (length) were generated. When injection rates of 10 and 7 mL/h were used, nucleation occurred after 12 and 20 min, respectively, and eventually producing MnP nanorods with sizes of 8 nm × 16 and 11 nm × 15 nm, respectively. On reducing the injection rate, more time was required in order to reach the critical Mn−TOP complex concentration necessary for nucleation, and consequently, nanorods with a lower aspect ratio were produced. In other words, the nucleation step is a critical determinant of MnP nanorod length control, because the Mn−TOP complex is stable and difficult to decompose for nucleation. On the contrary, the Fe−TOP complex was easily decomposed in 30 s to 1 min, and consequently, additional Fe−TOP complex added after nucleation decomposed to act as an effective growth source. Therefore, the growth step is important for Fe_2P nanorod length control, and the lengths of nanorods increased on decreasing the injection rate. When manganese acetylacetonate [$Mn(acac)_2$] was employed as a manganese precursor instead of $Mn_2(CO)_{10}$, no nanocrystals were produced, demonstrating that the metal precursor is critical for the successful synthesis of nanocrystals. According to a recent report by Brock and co-workers,[7a] when manganese carbonyl was reacted with $P(SiMe_3)_3$ (or trioctylphosphine) in trioctylphosphine oxide (TOPO)/myristic acid at 220 and 280 °C, spherical MnP nanoparticles with particles sizes of 5.1 and 6.7 nm were produced, respectively. These results demonstrate that the incorporation of a syringe pump plays a critical role in the formation of MnP nanorods instead of spherical nanoparticles.

When the Mn−TOP complex was injected into a solvent mixture composed of octyl ether and oleylamine, instead of TOPO, using a similar procedure, spherical MnO nanoparticles[10] were synthesized, as shown in Figure 2e,f, which demonstrates that the phosphine-rich environment achieved by the combined use of TOPO and TOP plays an important role in the synthesis of MnP nanorods. Furthermore, the formation of spherical MnO nanoparticles instead of rod-shaped MnP nanocrystals shows that the intrinsic crystal structure of the materials exerts a great influence on the morphology of the synthesized nanoparticles, because MnP has an anisotropic orthorhombic structure, whereas MnO has an isotropic cubic structure.[7a,10d]

Synthesis of Co_2P Nanorods. In the case of cobalt phosphide nanoparticles, the sizes and shapes of the nanoparticles were highly dependent on the stability of the metal−surfactant complexes used. Though the overall tendency was similar to that observed for the synthesis of the MnP nanoparticles, the change of length achieved by varying the injection rate was not significant. We used various surfactants in order to

(10) (a) Lee, G. H.; Huh, S. H.; Jeong, J. W.; Choi, B. J.; Kim, S. H.; Ri, H.-C. *J. Am. Chem. Soc.* **2002**, *124*, 12094. (b) Yin, M.; O'Brien, S. *J. Am. Chem. Soc.* **2003**, *125*, 10180. (c) Seo, W. S.; Jo, H. H.; Lee, K.; Kim, B.; Oh, S. J.; Park, J. T. *Angew. Chem., Int. Ed.* **2004**, *43*, 1115. (d) Park, J.; Kang, E.; Bae, C. J.; Park, J.-G.; Noh, H.-J.; Kim, J.-Y.; Park, J.-H.; Park, H. M.; Hyeon, T. *J. Phys. Chem. B* **2004**, *108*, 13598.

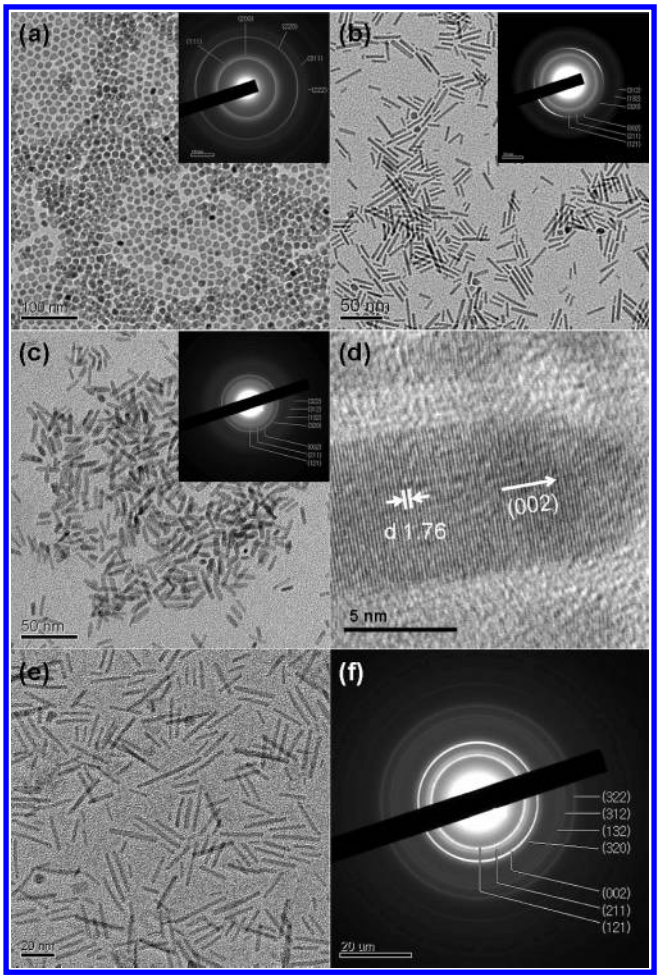

Figure 3. (a) TEM image of 11 nm sized spherical Co nanoparticles synthesized using $Co_2(CO)_8$, (b) TEM image of Co_2P nanorods with a dimension of 6 nm × 22 nm synthesized using $CpCo(CO)_2$, (c) normal TEM and (d) high-resolution TEM images of 5 nm × 20 nm sized Co_2P nanorods synthesized using $(Cp)_2Co$, (e) TEM image and (f) electron diffraction patterns of 2.5 nm × 20 nm sized Co_2P nanorods synthesized using $Co(acac)_2$ and hexadecylamine. Insets of panels a, b, and c are the corresponding ED patterns, respectively.

understand the effect of metal−surfactant complexes on the structures of nanoparticles. The Co−TOP and Co−oleylamine complexes, which were produced using $Co_2(CO)_8$ as the cobalt precursor, were so reactive that when the complexes were reacted at the temperatures above 250 °C, nanoparticles with mixed spherical and rod shapes were produced. When the reaction of these Co−TOP and Co−oleylamine complexes were performed at around 200 °C, nearly monodisperse 11 nm sized spherical cobalt nanoparticles with an fcc crystal structure were obtained, as shown in Figure 3a.[11] The cobalt−surfactant complexes prepared using cyclopentadienylcobalt dicarbonyl $[CpCo(CO)_2]$ as the precursor were more stable than those prepared using $Co_2(CO)_8$. When the cobalt−surfactant complexes were reacted in a mixed solvent composed of octyl ether and oleylamine at 300 °C using a syringe pump with an injection rate of 10 mL/h, Co_2P nanorods with average dimensions of 4 nm × 30 nm were predominantly produced with a small fraction of spherical nanoparticles (Figure 3b). When cobaltocene was employed as a precursor, Co_2P nanorods with a more uniform-size of 5 nm × 15 nm and improved crystallinity were obtained (Figure 3c,d). Cobalt acetylacetonate $[Co(acac)_2]$ formed a highly stable complex with TOP, and the reaction of the resulting Co−TOP complex in a mixed solvent (octyl ether and oleylamine) at 300 °C using a syringe pump generated Co_2P nanorods with a somewhat broad diameter distribution and average dimension of 5 nm × 35 nm. On the other hand, when the complex was reacted in a mixture solvent composed of octyl ether and hexadecylamine under similar conditions, uniformly sized 2.5 nm × 20 nm Co_2P nanorods were generated (Figure 3e,f). These results correspond with the fact that hexadecylamine induces the fabrication of thinner and longer nanorod, as Chaudret et al. suggested.[3b] Unlike the above experiments, when the cobalt−surfactant complexes were injected at once (without using syringe pump), polydispersed Co_2P nanoparticles with a size of 3−6 nm were produced (see the Supporting Information). From these results, we conclude that the syringe pump played an important role for preparing Co_2P nanorods.

Synthesis of FeP Nanorods. As we reported previously, when the Fe−TOP complex, which was prepared by reacting $Fe(CO)_5$ and TOP at 50 °C, was injected using a syringe pump in a mixed solvent composed of octyl ether and oleylamine at 300 °C, uniformly sized Fe_2P nanorods were produced.[9] Moreover, the sizes of the Fe_2P nanorods were controlled by varying the injection rates and by using various solvents.

When the Fe−TOP complex was added to TOPO at 360 °C using a syringe pump at 10 mL/h and then allowed to age at 360 °C for 30 min, uniform-sized FeP nanorods with an average dimension of 12 nm × 500 nm were produced (Figure 4a,b). When the reaction temperature was changed to 330 °C, FeP nanorods with an average dimension of 7 nm × 600 nm were obtained (Figure 4c). As we reported earlier, when we substituted oleylamine for TOPO using a very similar procedure, uniform-sized Fe_2P nanorods were produced.[9] These results show that the selection of the stabilizing surfactants determined whether the FeP or the Fe_2P phase is produced. It seems that the phosphorus-rich environment associated with the combined use of TOPO and TOP promoted the formation of FeP. Liu and co-workers reported that multiple injections of the Fe−TOP complex into TOP/TOPO at high temperature produced FeP nanorods and nanowires.[8] Recently, Chi and coworkers reported the synthesis of iron phosphide nanowires via the thermal decomposition of (cyclohexadiene)iron tricarbonyl in TOP/TOPO mixture solvent at 340 °C.[12]

Synthesis of Ni_2P Nanorods. Nickel phosphide (Ni_2P) nanorods were synthesized successfully by thermally decomposing the Ni−TOP complex, which was synthesized by reacting acetylacetonate $[Ni(acac)_2]$ and TOP using a syringe pump at an injection rate of 10 mL/h. TEM, HRTEM, and electron diffraction images revealed that highly crystalline Ni_2P nanorods of dimension 4 nm × 9 nm and with a triangular prismlike structure were produced (Figure 5), but when nickelocene was employed as the precursor, ill-shaped, nonuniformly sized nanoparticles were obtained.

On the basis of the results described above, we proposed the following mechanism for the nanorod formation (Scheme 1). The formation of 1-D nanorods seems to be caused by the cooperative effects from both the different binding capability of two surfactants (TOP and oleylamine) and intrinsically anisotropic crystal structures of the phosphides (orthorhombic

(11) Petit, C.; Taleb, A.; Pileni, M. P. *J. Phys. Chem. B* **1999**, *103*, 1805.

(12) Chen, J.-H.; Tai, M.-F.; Chi, K.-M. *J. Mater. Chem.* **2004**, *14*, 296.

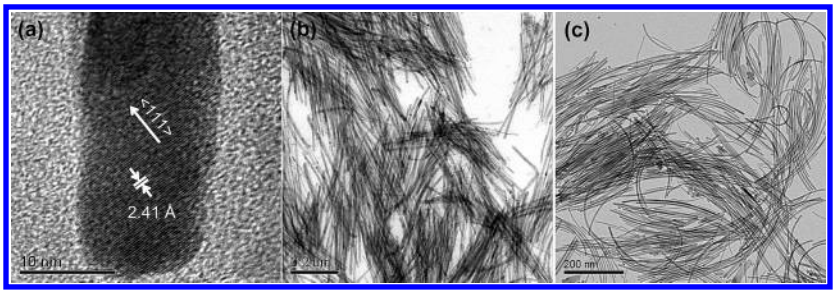

Figure 4. (a) High resolution and (b) normal TEM images of 12 nm × 500 nm sized FeP nanowires and (c) normal TEM images of 7 nm × 600 nm sized FeP nanowires.

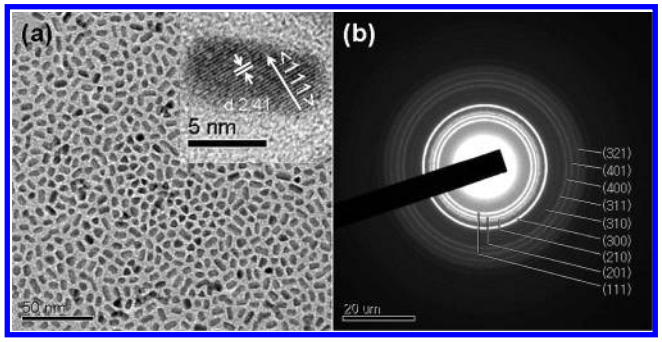

Figure 5. (a) Normal TEM image and (b) electron diffraction patterns of Ni_2P nanorods. The inset is a high-resolution TEM image.

Scheme 1. Proposed Growth Mechanism for Nanorod Formation

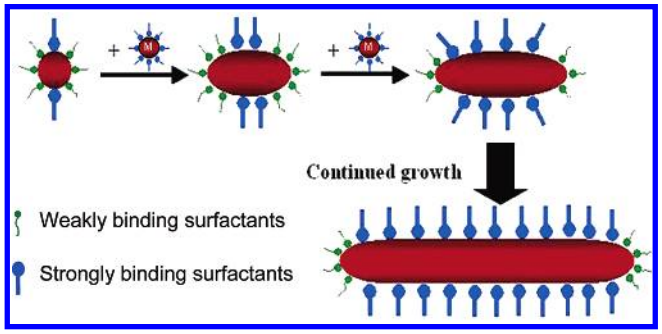

for MnP, Co_2P, and FeP and hexagonal close packed for Ni_2P). When the amount of metal−TOP complex injected reached above a critical point, nucleation took place. After the initial formation of spherical nanoparticles, growth subsequently occurs on these nanospheres along preferential direction, because strongly binding TOP surfactants seem to preferentially bind to the crystal growth face. For example, in the case of Co_2P nanorods, the direction of the crystal growth was perpendicular to (002).

To understand the one-dimensional growth mechanism of FeP nanorods, we conducted the following supplementary experiments (see the Supporting Information). First, to understand the role of the TOP surfactant in the growth of the nanorods, we systematically changed the relative amount of TOP, while all the other experimental parameters remained unchanged (injection rate, 10 mL/h; aging temperature, 330 °C; aging time, 1 h). When 10 mL of TOP was used in the synthesis, predominantly 7 nm × 600 nm sized nanorods were generated. When the amount of TOP in the stock solution was decreased to 8 mL, 14 nm × 500 nm sized nanorods were generated. When the amount of TOP in the stock solution was further decreased to 5 mL, nearly spherical nanoparticles were generated, and no nanorods were produced. When less than 5 mL of TOP was used in the synthesis, an insoluble coalescence of the nanoparticles was observed, and ultimately in the absence of TOP, using 1-octadecene as noncoordinating solvents in stock solution, irregularly shaped nanoparticles were formed (see the Supporting Infomation). These results demonstrate that an optimum amount of TOP is required for the preferential growth along the ⟨002⟩ direction by stabilizing crystal faces perpendicular to (002). Second, we have taken TEM images of the aliquots from the reaction mixture for the synthesis of 7 nm × 600 nm sized FeP nanorods at the various stages of the synthesis (TEM images are shown in the Supporting Information). The TEM image of the aliquot taken after injecting Fe−TOP complex into the TOPO solution at 330 °C for 15 min showed that short nanorods (∼4 nm × 15 nm) along with small spherical nanoparticles (∼4 nm) were generated. As the injection of the Fe−TOP was further proceeded, the lengths of the nanorods became longer and the diameters became thicker (from 4 to 7 nm). These results demonstrate that a kind of seed-mediated growth mechanism seems to work in our current synthesis of nanorods, as we proposed in the Scheme 1.[13]

Structural and Magnetic Characterization of Metal Phosphide Nanorods. To characterize the crystal structures of these metal phosphide nanorods, we collected X-ray diffraction (XRD) patterns. The XRD patterns of MnP, Co_2P, and FeP nanorods, shown in Figure 6, revealed an orthorhombic crystal structure, which is the bulk crystal structure of the corresponding metal phosphides. The XRD of Ni_2P nanorods revealed a bulk hexagonal crystal structure. To show the growth direction of the nanorods directly, we obtained HRTEM images of the nanorods (Figure 7). The HRTEM images clearly show the lattice plane perpendicular to the growth direction. The results were also confirmed by the relative peak widths (intensity) in the XRD patterns. In summary, the XRD and HRTEM studies showed that the MnP and Co_2P nanorods grow perpendicular to the (002) planes, FeP nanowires grow perpendicular to the (013) planes, and Ni_2P nanorods grow perpendicular to the (300) planes.

To understand the magnetic properties of these nanorods, we investigated the temperature and field dependences of magnetization, using a commercial superconducting quantum interference device (SQUID) magnetometer. One of the main motivations for our magnetization studies is a well-accepted experimental view that the magnetic properties of nanoparticles are nontrivial and cannot always be expected simply on the basis of what is

(13) (a) Murphy, C. J.; Jana, N. R. *Adv. Mater.* **2002**, *14*, 80. (b) Gole, A.; Murphy, C. J. *Chem. Mater.* **2004**, *16*, 3633. (c) Gao, J. X.; Bender, C. M.; Murphy, C. J. *Langmuir* **2003**, *19*, 9065. (d) Nikoobakht, B.; El-Sayed, M. A. *Chem. Mater.* **2003**, *15*, 1957. (e) Johnson, C. J.; Dujardin, E.; Davis, S. A.; Murphy, C. J.; Mann, S. *J. Mater. Chem.* **2002**, *12*, 1765. (f) Jana, N. R.; Gearheart, L.; Murphy, C. J. *Adv. Mater.* **2001**, *13*, 1389. (g) Jana, N. R.; Gearheart, L.; Murphy, C. J. *Chem. Mater.* **2001**, *13*, 2313.

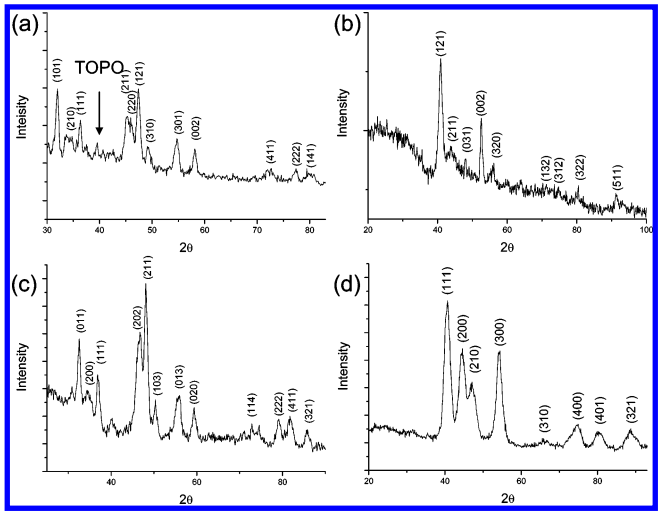

Figure 6. X-ray diffraction patterns of (a) MnP nanorods, (b) Co_2P nanorods, (c) FeP nanowires, and (d) Ni_2P nanorods.

already known for bulk samples. Thus, we believe that it is a reasonably good, and sometimes well-rewarding, practice to examine the magnetic properties of all nanoparticles, which is demonstrated by our findings as subsequently discussed. For field dependence measurements, we cooled the samples to a target temperature under a zero-field condition from well above the so-called sample blocking temperatures. Magnetization temperature dependences were measured from 2 to 380 K, while being warmed with an applied field of 100 Oe after both zero-field cooling (ZFC) and field cooling (FC) from 380 K.

Figure 8 shows the temperature dependence of magnetization for (b) 4 nm × 35 nm Co_2P and (c) 4 nm × 9 nm Ni_2P measured after zero-field cooling (filled circles) and field cooling (open circles). For comparison, the temperature dependence of magnetization is also shown for (a) 5 nm × 45 nm Fe_2P taken from ref 9. As shown in Figure 8, neither Co_2P nanorods nor Ni_2P nanorods exhibited any evidence of a temperature dependence anomaly, although the Fe_2P nanorods showed a maximum in the ZFC magnetization, i.e., blocking temperature (T_B). The difference between the temperature dependences of samples was also consistent with the field dependence of the magnetization, as shown in the insets. Unlike Fe_2P, which displays hysteresis behavior below the blocking temperature, no such anomaly was seen during the magnetization of Co_2P and Ni_2P nanorods, within the resolution of our experiments. Another interesting point is that although bulk Co_2P and Ni_2P are known to be Pauli paramagnetic,[14a] our Co_2P and Ni_2P nanorods showed Curie−Weiss behavior[14b] between 200 and 380 K with the Curie−Weiss temperature $\Theta_{CW} = -368$ and -364 K, while the effective moments are estimated to be 467 and 334 μ_B/fu, respectively (see the Supporting Information). The large effective moments are reasonable, as we expect that a single nanoparticle or at least some significant part of it plays as a single giant magnetic moment at high temperatures, i.e., superparamagnetic behavior. At the same time, the nanoparticles have strong magnetic interactions between them, as indicated by the large Curie−Weiss temperature. Our experimental observations suggest that the Co_2P and Ni_2P nanorods have magnetic properties different from their bulk counterparts: for comparison, both samples are Pauli paramagnets with almost

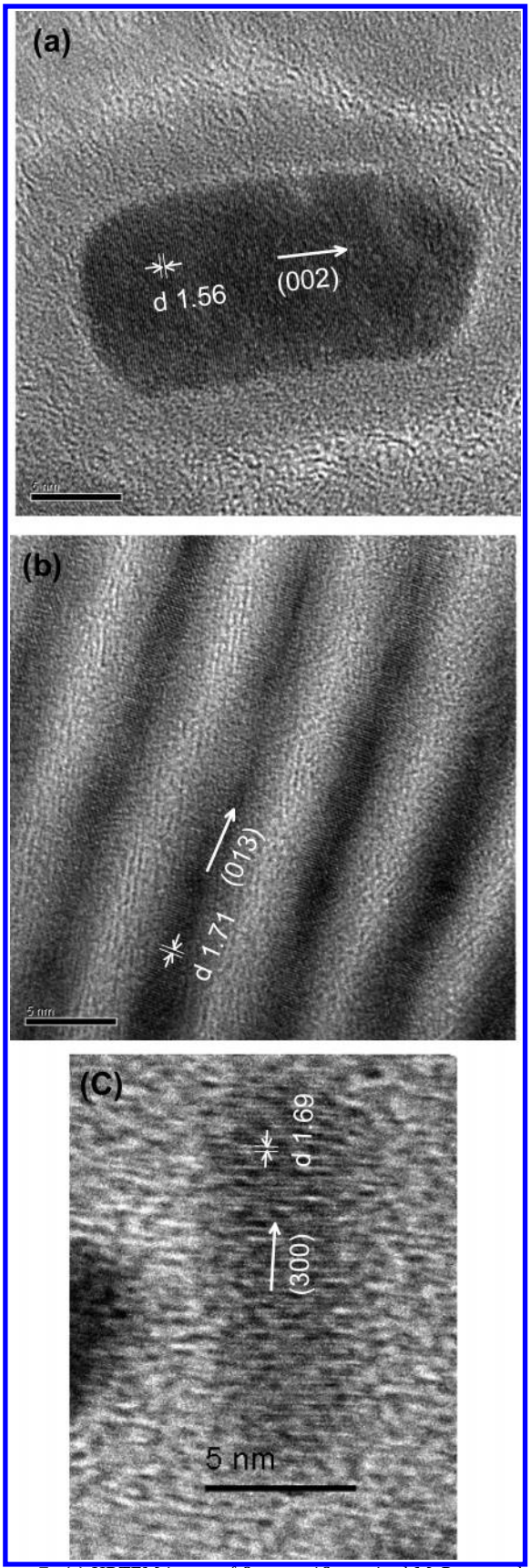

Figure 7. (a) HRTEM image of 8 nm × 16 nm sized MnP nanorod. (b) HRTEM image of 7 nm × 600 nm sized FeP nanorod. (c) HRTEM image of 4 nm × 9 nm sized Ni_2P nanorod.

(14) (a) Fujii, S.; Ishida, S.; Asano, S. *J. Phys. F: Met. Phys.* **1988**, *18*, 971. (b) Ohta, S.; Onmayashiki, H. *Physica B* **1998**, *253*, 193.

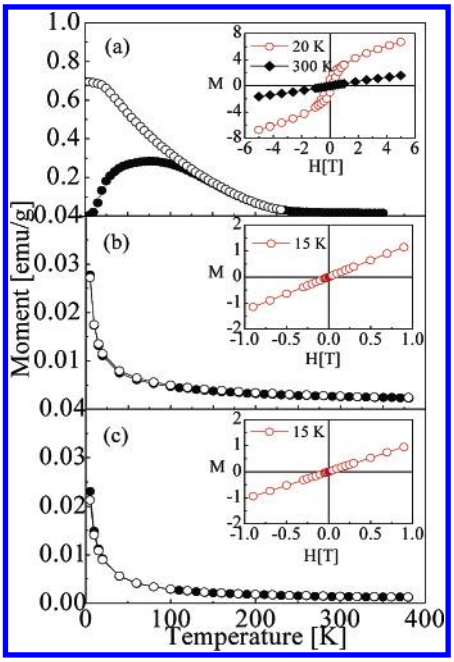

Figure 8. It shows the temperature dependence of magnetization for (a) 5 nm × 45 nm Fe_2P, (b) 4 nm × 35 nm Co_2P, and (c) 4 nm × 9 nm Ni_2P measured after zero-field cooling (filled circles) and field cooling (open circles) with an applied field of 100 Oe. The inset displays the field dependence of the magnetization at base temperature. We show the data for Fe_2P taken from ref 9 in order to demonstrate how the magnetic properties evolve on going from Fe to Co to Ni.

no temperature dependence of the susceptibility in bulk forms. We admit that it is not easy to imagine how such a giant moment state can arise from a Pauli paramagnetic state, although there are several examples in which some nanoparticles have magnetic states different from those of bulk samples through some kind of surface state. To some extent, we speculate that such a surface magnetic state is likely to play a certain role in the magnetic properties of our Co_2P and Ni_2P nanorods.

We have also studied the magnetic properties of two MnP nanorod samples (8 nm × 16 nm and 11 nm × 25 nm) and one FeP sample (11 nm × 450 nm). Because we obtained similar results for the two MnP nanorods with different sizes, we only showed the results of the MnP nanorods with a size of 11 nm × 25 nm together with the data for the FeP nanorods in Figure 9. Both samples showed relative high blocking temperatures—$T_B = 260$ K for the MnP nanorods and $T_B = 350$ K for the FeP nanorods—and this temperature dependence agreed with the field dependence of the magnetization, as shown in the insets. Fe_2P nanorods of dimension 6 nm × 300 nm had a T_B of 236 K, lower than the T_B of the FeP nanorods. The extremely large coercive field found in both samples—at 15 K, Hc = 5 kOe for MnP and Hc = 8.2 kOe for FeP—is of particular interest. For comparison, we found Hc = 3.9 kOe for 5 nm × 45 nm sized Fe_2P nanorods at 2 K and about 8.3 kOe for FeP nanorods at the same temperature. We note that bulk FeP is known to have an antiferromagnetic transition temperature with a Neel temperature (T_N) of 115 K,[15] whereas bulk MnP has a ferromagnetic transition temperature (T_c) of 291.5 K.[16] Our results seem to be consistent with recent studies on MnP nanospheres, which

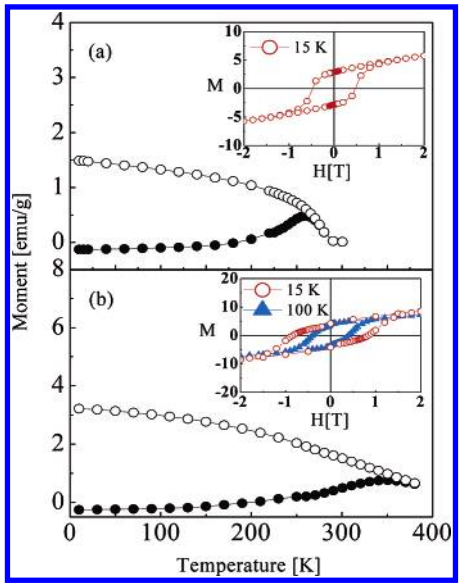

Figure 9. The temperature dependence of magnetization for (a) 11 nm × 25 nm MnP and (b) 11 nm × 450 nm FeP sample measured with an applied field of 100 Oe after zero-field cooling (filled circles) and field cooling (open circles). The inset displays the field dependence of the magnetization of (a) MnP at 15 K and (b) FeP at 15 and 100 K.

showed that 5.1 and 6.7 nm sized spheres have blocking temperatures of 60.8 and 74.3 K with reasonably large coercive fields, respectively.[17]

Therefore, the magnetic properties of FeP were strongly dependent on whether it was in the bulk or nanoparticle form. The large coercive field found in our FeP nanoparticles is another piece of evidence that supports our conclusion that their magnetic properties are remarkably different from those of the bulk FeP. Similar observation has been made on NiO, although bulk NiO is an antiferromagnet[18] and the unusually large coercive field in NiO nanoparticles was ascribed to the effects of uncompensated spin on surface moments. We also note that a recent report[19] on 5 nm FeP nanoparticles showed no blocking behavior and zero coercive field, which implies that the magnetic properties of FeP are sensitive to particle size and shape. On balance, we acknowledge that it is still difficult to believe such a drastic change can occur to the magnetic properties of FeP upon reducing the size. Instead, one may be easily tempted to ascribe the observed behavior to a small amount of Fe impurity present either outside or inside of FeP nanorods. For example, the saturated magnetic moment of 350 emu/mol at 15 K found for our FeP nanorods can be accounted for by about 1 wt % of Fe. We admit that this explanation cannot be entirely disregarded, although our HRTEM as well as XRD did not find any evidence of pure Fe in our samples. Finally, we would like to point out that according to our long experience with Fe it is easily oxidized under harsh environments like ours and unlikely to exist as pure Fe nanoparticles in our samples.

A further interesting point was found in the temperature dependence of the coercive field for the four different samples,

(15) (a) Felcher, G. P.; Smith, F. A.; Bellavance, D.; Wold, A. *Phys. Rev. B* **1971**, *3*, 3046. (b) Haggstrom, L.; Narayanasamy, A. *J. Magn. Magn. Mater.* **1982**, *30*, 249.
(16) Huber, E. E., Jr.; Ridgley, D. H. *Phys. Rev.* **1964**, *135*, A1033.
(17) Perera, S. C.; Tsoi, G.; Wenger, L. E.; Brock, S. L. *J. Am. Chem. Soc.* **2003**, *125*, 13960.
(18) (a) Chikazumi, S. *Physics of Ferromagnetism*, 2nd ed.; Clarendon Press: Oxford, 1997. (b) Kodama, R. H.; Makhlouf, S. A.; Berkowitz, A. E. *Phys. Rev. Lett.* **1997**, *79*, 1393.
(19) Perera, S. C.; Fodor, P. S.; Tsoi, G. M.; Wenger, L. E.; Brock, S. L. *Chem. Mater.* **2003**, *15*, 4034.

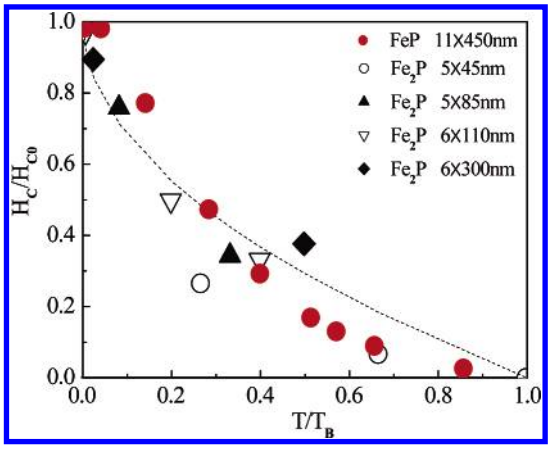

Figure 10. Normalized coercive field (Hc/Hc_0) is plotted for a normalized temperature (T/T_B) for five different FeP and Fe_2P samples, where Hc_0 is an estimated coercive field at $T = 0$ K and T_B is the measured blocking temperature of each sample. The line is for the theoretical curve for a single domain of fine particles (see the text).

as shown in Figure 10. The line is a theoretical curve for single-domain fine particles:[20] $Hc/Hc_0 = 1 - (T/T_B)^{1/2}$, where Hc is the measured coercive field, Hc_0 the estimated coercive field at $T = 0$ K, and T_B the measured blocking temperature. Although we acknowledge that there is some discrepancy between the data points and the theoretical line, it is reasonable to say that the temperature dependence of the measured coercive fields of the four different samples can be accounted for by the simple theoretical curve for a single domain of fine particles.

(20) Cullity, B. D. *Introduction to magnetic materials*; Addison-Wesley: Reading, PA, 1972.

Conclusions

In summary, we synthesized uniformly sized metal phosphide nanorods of manganese, iron, cobalt, and nickel by the thermal decomposition of the continuously delivered metal−surfactant complexes via a syringe pump. The current synthetic procedure is simple and highly reproducible. We have found that the method has general applicability and that nanorods of many transition metal phosphides could be synthesized. Moreover, these nanorods exhibited interesting magnetic properties, which are significantly different from those of their bulk counterparts. We believe that this new synthetic procedure can be used to synthesize nanorods of many other materials.

Acknowledgment. T.H. would like to thank the National Creative Research Initiative Program of the Korean Ministry of Science and Technology for the financial support. Works at Sungkyunkwan University were supported by the Proton Accelerator User Program (No. M102KS010001-02K1901-01810) of the Proton Engineering R & D Project and the Center for Strongly Correlated Materials Research.

Supporting Information Available: TEM images and ED patterns of Co_2P and MnP nanoparticles synthesized without using a syringe pump, TEM images of the FeP nanorods prepared using different amounts of TOP, TEM images of aliquots taken from the reaction mixture for the synthesis of FeP nanorods at various reaction time intervals, and inverse susceptibility data for Co_2P and Ni_2P. This material is available free of charge via the Internet at http://pubs.acs.org.

JA0427496